ELSEVIER

Earth and Planetary Science Letters 143 (1996) 81–94

EPSL

Petrological models of magma evolution and deep crustal structure beneath hotspots and flood basalt provinces

Cinzia G. Farnetani [a,*], Mark A. Richards [a], Mark S. Ghiorso [b]

[a] *University of California at Berkeley, Department of Geology and Geophysics, Berkeley, CA 94720-4767, USA*
[b] *University of Washington, Department of Geological Sciences, AJ-20, Seattle, WA, 98195, USA*

Received 3 January 1996; accepted 9 July 1996

Abstract

Seismic experiments imaging the deep crustal structure beneath hotspot tracks and oceanic plateaus indicate unusually high seismic velocities ($V_P = 7.3–7.8$ km/s) at the base of the crust. These high-velocity 'layers', up to 10 km thick, are generally interpreted as large igneous intrusions. In this paper we investigate the extent to which plume magmatism affects the crust, and propose a model for the origin and composition of the high-velocity layers. We use the petrological code MELTS [1] to quantify the evolution of primary mantle melts as they ascend to the surface along an imposed pressure–temperature path. Crystal fractionation is an important process for plume volcanism, as suggested by the discrepancy between the composition of the erupted lavas, predominantly tholeiitic basalts, and the expected picritic composition of the parental mantle melts. In our model the initial liquid compositions are taken from melting experiments on spinel lherzolites at 10–30 kbar pressure and span reasonable compositional differences over a depth range of melting. MELTS rigorously calculates the amount and composition of the fractionated solid phases and the major oxide concentration of the residual liquid. For picritic initial liquid compositions (i.e., those formed at 30 and 20 kbar pressure) our petrological model predicts a distinct crustal structure: at the base of the crust (e.g., at $P = 3$ kbar) the fractionated cumulates are olivine and augitic pyroxene, with variable amounts of plagioclase. The calculated compressional wave velocities of the cumulates are 7.5–7.9 km/s. In the upper crust ($P = 1$ kbar) intrusions are olivine gabbros ($V_P \sim 7.0$ km/s). We also find that the coexistence of high-velocity layers at the base of the crust, with high upper crustal velocities is diagnostic of deep (30–20 kbar pressure) melting. Our results indicate that the lower-crustal high-velocity layers beneath oceanic plateaus and hotspot tracks represent fractionated cumulates from picritic mantle melts and are therefore an integral part of plume volcanism. This conclusion suggests that high-velocity layers should be present also beneath continental flood basalt provinces.

Keywords: plumes; crust; high-velocity zones; picrite; tholeiitic basalt; models; melts

1. Introduction

The interpretation of crustal structure in provinces affected by plume volcanism requires an understanding of the geodynamic and petrologic processes associated with partial melting of mantle plumes. Plumes of hot material rising from the Earth's mantle are thought to cause intraplate volcanic hotspots [2]. It is also likely that continental flood basalts and oceanic plateaus were formed by enhanced melting of a large plume head at the initiation of mantle plume activity [3–5]. Geochemical analyses of flood basalts provide

* Corresponding author. Present address: Dept. Terre–Atmosphere–Ocean, Ecole Normale Supérieure, 24, rue Lhomond, 75231 Paris 05, France. E-mail: cinzia@geophy.ens.fr

PII S0012-821X(96)00138-0

constraints on the depth of primary melting for plume magmatism, and often indicate that garnet-bearing peridotite is a likely magma source. A garnet-bearing source has been suggested for Hawaii [6], for the Siberian Traps [7], and for the Wrangellia Terrane [8], which is probably an accreted fragment of an oceanic plateau [9].

Thermomechanical models of plume–lithosphere interaction indicate that melting of the lithosphere is minimal and that the bulk of primary magmas are produced within the mantle plume [10,11]. The estimated melting depth of 70–120 km (i.e., 20–40 kbar pressure) is within the stability field of garnet peridotite. According to petrological models and melting experiments on mantle lherzolite in this pressure range, the composition of the liquid is picritic, with high MgO content (15–18 wt%). Although picrites occur in provinces affected by plume magmatism, the largest volumes of volcanic rocks are tholeiitic basalts, with a fairly constant MgO concentration (6–8 wt%).

The discrepancy between the predicted composition of the primary melt at depth and the observed composition of the erupted lavas indicates that primary mantle melts undergo significant crystal fractionation before being erupted. The conclusion that erupted lavas do not represent primary magmas, but are instead largely derived via crystal fractionation, has important implications for crustal evolution [12]. Fractionated cumulates and intrusions would cause underplating and thickening of the crust, and these features should be detectable by geophysical observations.

There is now a growing body of seismic data that allow imaging of the deep crustal structure of hotspot tracks, such as Hawaii [13] and the Marquesas Islands [14], of oceanic plateaus, such as Ontong Java [15], and of continental flood basalt provinces, such as the Columbia River Plateau [16]. The seismic data consistently indicate crustal thickening and the existence of high-velocity layers at the base of the crust. These layers are a few kilometers thick (up to 10 km), and their seismic velocities are intermediate between those of the mantle and those typical of the lower crust.

In this paper we investigate the effect of plume magmatism on the crustal structure beneath hotspots and oceanic plateaus, and we provide a model for the origin of the high-velocity layers often detected at the base of the crust. We study the petrological evolution of picritic mantle melts using MELTS [1], a code for fractionation/assimilation processes in silicate liquids. MELTS is based on a rigorous thermodynamic formulation of liquid- and solid-phase equilibria, and it calculates the composition and amount of liquid and solid phases as a function of pressure, temperature and initial liquid composition.

In our models crystal fractionation is the dominant process through which picritic melts evolve toward a basalt. The initial liquid compositions are taken from recent melting experiments on spinel lherzolites at 10, 20 and 30 kbar pressure [17], and hopefully bracket a possible range of mantle melt compositions. The pressure–temperature paths are chosen assuming rapid magma transport along the liquid adiabat, followed by major cooling and fractionation at constant pressure. Crystal fractionation occurs predominantly at the base of the crust, since the Moho may represent a density [18] and/or a rheological [19] trap that inhibits the ascent of partial melts. We explore a range of Moho depths (10–17 km) which are appropriate to the oceanic environment. We then compare the crustal velocities structure observed beneath oceanic plateaus and hotspots with the compressional wave velocities calculated for the fractionated cumulus and for upper crustal intrusions. Similarly, the composition of basaltic lavas from oceanic plateaus is compared to the calculated major oxide concentrations of the evolved liquids.

Our results show that crystal fractionation of picritic primary melts (i.e., those formed at 20 and 30 kbar) generates mafic cumulus at the base of the crust, with calculated seismic velocities of 7.5–7.9 km/s. Intrusions in the upper crust are gabbros, variably enriched in olivine, with velocities of 7.0–6.8 km/s. In contrast, fractionation of shallow primary melts (i.e., using the 10 kbar initial composition) generates gabbros, variably enriched in orthopyroxene, with seismic velocities of 7.2–6.8 km/s.

As expected primary melts generated at higher pressure have higher normative olivine contents, therefore fractionation at shallow depths results in olivine rich (thus seismically fast) cumulates. For mantle plume magmatism we can reconcile the ex-

pected picritic composition of mantle melts with the observed basaltic composition of the erupted lavas only if significant fractionation occurs. We suggest that the high-velocity layers observed at the base of the crust are genetically related to plume magmatism, being mafic cumulates of olivine, augitic pyroxene and some plagioclase formed during crystal fractionation of picritic mantle melts. Our models also indicate that important volumes of cumulates and intruded rocks accompany surface volcanism.

2. Modelling approach

2.1. Petrological calculations

We use the thermodynamic code MELTS [1] to model fractional crystallization for a multicomponent system. MELTS finds the composition of the liquid and solid phases at equilibrium at a given pressure, temperature and liquid composition, by minimizing the Gibbs free energy of the system. The model treats the irreversible process of magmatic crystallization as a series of steps, each characterized by thermodynamic equilibrium, providing a rigorous description of the bulk chemical effects which accompany crystallization. At each step of the imposed pressure–temperature path, the code calculates the composition and the amount of the solid phases fractionated and the composition of the residual liquid.

The bulk of the constraints used to calibrate MELTS are from low pressure experiments, however the experimentally measured volumes, thermal expansivities and compressibilities allow extrapolation to high pressure [20,21]. At 10 kbar MELTS reproduces well the shape and trends of recent melting experiments [22], although there is a systematic discrepancy between observed and calculated concentrations for some oxides (e.g., SiO_2). We avoid modeling the whole fractionation path from the source region to the surface and we restrict our calculations to the pressure range where MELTS is accurate.

The initial composition of the primary melt is from anhydrous melting experiments on natural spinel lherzolites by Hirose and Kushiro [17]. Although partial melting in a mantle plume occurs over a depth range, we consider for simplicity three initial compositions formed at constant pressure. The composition of the partial melts formed at 30, 20 and 10 kbar (hereafter called IC-30, IC-20 and IC-10, respectively) are shown in Table 1. Their corresponding melt fractions are 16.6, 13.5 and 12.1 wt% (Table 4 of [17]). These melt fractions are higher than what is expected for fractional melting in the mantle; however, at present there are no experiments that directly constrain the compositions of near-solidus melts at high pressure. Recent experiments at 10 kbar show that near-solidus melts are enriched in SiO_2, Al_2O_3, Na_2O, and depleted in FeO, MgO, CaO, relative to higher melt fraction [22].

Table 1
Initial composition of partial melts

Oxide	IC-30	IC-20	IC-10
SiO_2	45.65	47.53	50.45
TiO_2	0.99	0.75	0.65
Al_2O_3	14.31	15.55	17.96
FeO_{tot}	9.64	8.57	6.71
Cr_2O_3	0.21	0.21	0.11
MgO	16.71	13.96	10.09
CaO	10.62	11.12	11.38
Na_2O	1.80	2.22	2.47
K_2O	0.07	0.08	0.09

We use the mass and composition of the fractionated minerals to calculate the compressional wave velocity of the fractionated assemblage. For each mineral we consider an upper and a lower compressional wave velocity [23] to account for variations in the mineral composition (Table 2), since higher FeO content decreases the seismic velocities. The upper and lower compressional velocities for the solid assemblage are then calculated as the sum of each mineral velocities (upper and lower, respectively), weighted by the relative volume percent of each mineral. We note that the calculated velocities of the solid assemblage may differ from in situ seismic velocities, since compressional velocity increases with lithostatic pressure (i.e., $dV_P/dP \sim 1\text{–}1.5 \times 10^{-2}$ km s^{-1} kbar^{-1}) and decreases with temperature (i.e., $dV_P/dT \sim 2\text{–}6 \times 10^{-4}$ km s^{-1}°C^{-1}) ([25], and references therein).

2.2. Magma evolution paths

In our models primary mantle melts rise along their liquidus from the melting region to the base of

the crust. The implicit assumption is that partial melts rise rapidly in the uppermost mantle, probably through veins and cracks, without undergoing significant cooling and fractionation. Consequently the composition of the melts reaching the Moho is the same as the initial composition of the primary melts given in Table 1. We consider that the crust/mantle boundary may act as a barrier to the ascents of mantle melts, inducing ponding at the base of the crust. We have investigated a range of initial pressures of crystallization, at $P = 3$ kbar (corresponding to a Moho depth of $\sim$ 10 km, appropriate for typical oceanic crust), and $P = 5$ kbar (Moho depth of $\sim$ 17 km, appropriate for thickened oceanic crust).

We also consider two possible cases. For the 'one stage case' fractionation occurs exclusively at the Moho, which implies rapid magma transport from the reservoir to the surface without significant crystal fractionation. For the Columbia River basalts physical and chemical constraints require that the flows were fed from a large magma reservoir near the crust–mantle boundary and indicate that no significant crystal fractionation and assimilation occurred between reservoir and surface [25]. For the 'two stage case' fractionation occurs in part at the Moho and in part at shallower pressure. The likelihood of polybaric fractionation for some flood basalt lavas has been suggested by Cox [12], based on petrological observations. In our model the pressure of shallow level fractionation is $P = 1$ kbar ($\sim$ 3.5 km), which is consistent with the depth of magma chambers seismically imaged under the Kilauea volcano in Hawaii [26].

The Moho has often been suggested as a locus of magmatic underplating. However, the physical conditions that cause a picritic mantle melt to pond and form sills at the base of the crust are unclear. To define the forces that cause spreading and ponding at the Moho requires an understanding of how magmas rise from the mantle to the surface. It is generally assumed that lithostatic load and magma density have a major effect on whether magma will reach the surface or will ascend only to some equilibrium position. Picritic melts rise in the mantle in response to buoyancy forces, and they may flow laterally at the base of the crust if their density is intermediate between that of the crust and of the mantle (e.g. [18]).

A likely mechanism to transport large quantities of hot magma is through fractures, in this case the level of the top of the magma column is determined by the weight of the magma column and by the overburden pressure acting in the source region [27]. The overburden pressure depends on the thickness of the crust and on the depth of the source. For a dike to advance upwards the fluid pressure at the top of the column must exceed the lithostatic pressure. If the melt is present in continuous conduits down to a magma chamber it is the *integrated* density contrast, rather than the local density contrast, that controls whether the melt will rise. In this case dense melts can ascend through less dense surrounding rocks. These models are probably considerable simplifications of the natural system and neglect the effect of rheological differences within the crust and the upper mantle. Parsons et al. [19] show that the viscosity increase between the lower crust and the mantle affects the orientation of the greatest and least principal stress axes, so that horizontal intrusions and ponding may be favored at a rheological boundary. Moreover, if the host rocks are sufficiently elastic to support differential tectonic stresses, the density of the surrounding rocks is less important, suggesting that variations in horizontal stresses, rather than

Table 2
Compressional wave velocity and density of minerals

Mineral	$V_{P_{max}}$ (km/s)	$V_{P_{min}}$ (km/s)	Density (g/cm^3)
Olivine ($Fo_{90}Fa_{10}$–$Fo_{75}Fa_{25}$)	8.35	8.15	3.33
Clinopyroxene (augite)	7.70	7.40	3.33
Orthopyroxene ($En_{95}Fs_5$–$En_{80}Fs_{20}$)	7.80	7.60	3.33
Plagioclase ($An_{75}Ab_{25}$–$An_{65}Ab_{35}$)	6.70	6.40	2.65
Spinel	9.10	9.00	4.20

host-rock density may control the behavior of tabular intrusions [19].

Given the complexity of the problem it is clear that the models used for our calculations are only rough approximations of the pressure–temperature path for mantle melts rising to the surface.

3. Results

We are particularly interested in modeling the effect of plume magmatism in an oceanic environment and in understanding the crustal structure detected beneath some oceanic plateaus and hotspot

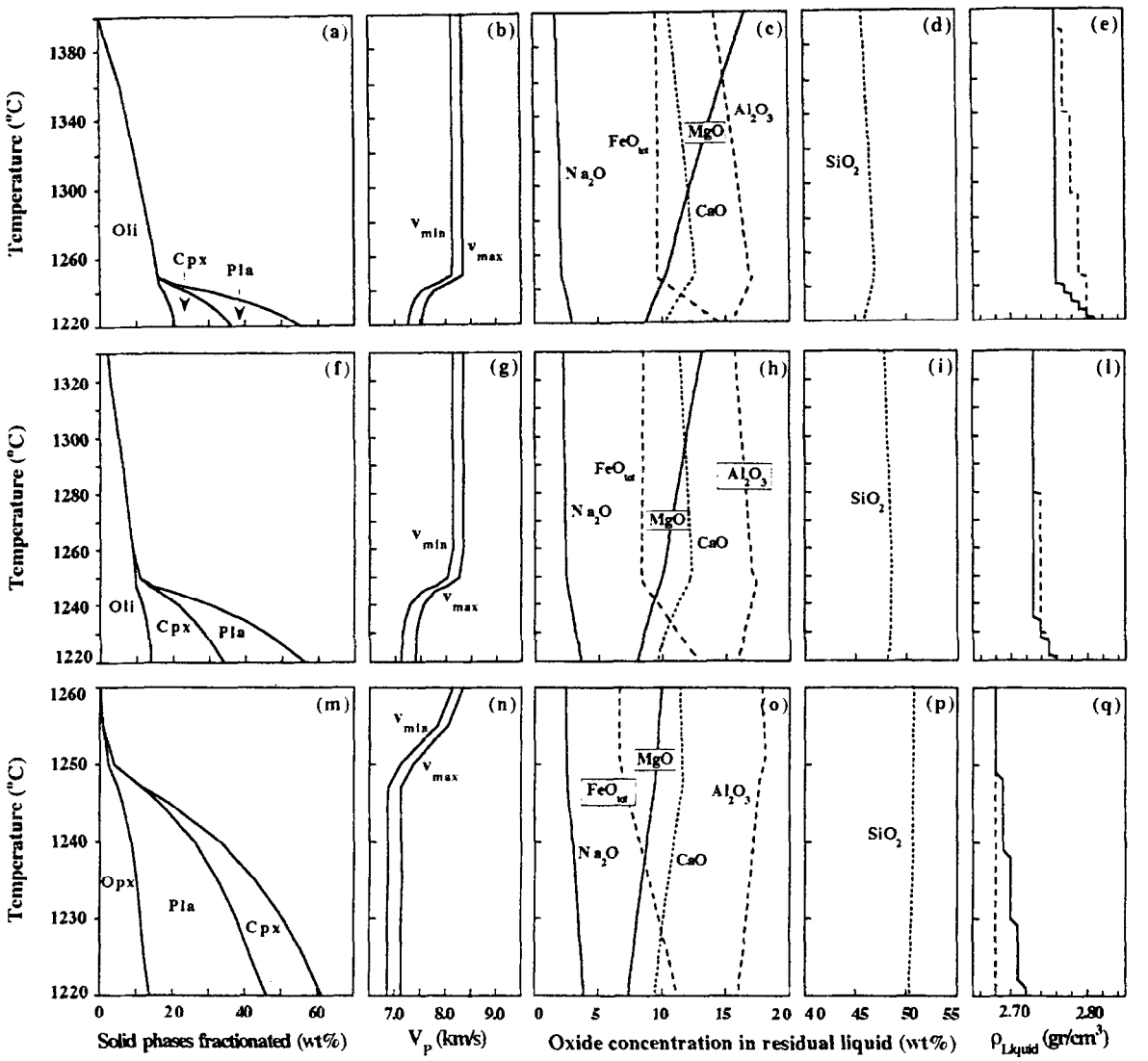

Fig. 1. Fractional crystallization at $P_{Moho} = 3$ kbar for initial composition IC-30 (top), IC-20 (middle), IC-10 (bottom). Temperature vs.: (a,f,m) solid phases fractionated. For graphical reasons spinel is not shown, its maximum weight fraction is 0.8–0.5%. (b,g,n) Compressional velocity of solid phases. (c–d,h–i,o–p) Major oxide concentration in the liquid. (e,l,q) Liquid density of the residual liquid (solid line) and of a liquid with constant initial composition (dashed line). The step increments of 0.01 g/cm^3 correspond to the minimum density increment calculated by MELTS.

tracks. Since the oceanic crust is thinner and has a more mafic composition compared to the continental crust, we can at first ignore assimilation processes. We model fractional crystallization, which implies that the crystals segregate from the residual liquid as soon as they form.

3.1. Moho at $P = 3$ kbar

The results for the initial composition IC-30 are shown in the top panels of Fig. 1. Fig. 1a shows the sequence and the cumulative amount of fractionated minerals as the temperature decreases from the liquidus to 1220°C. Olivine is followed at lower temperature by augite and plagioclase, as predicted by the Bowen series. The seismic velocity for the cumulates (Fig. 1b) ranges from 8.5 to 7.5 km/s, reflecting the high content of olivine. Fig. 1c and d show the composition of the residual liquid. The most pronounced effect of olivine fractionation is the decrease in MgO, while SiO_2 is approximately constant. Fractionation of augite and plagioclase enriches the residual liquid in FeO_{tot}, and depletes it in CaO, Al_2O_3 and SiO_2. These major oxide variations are in agreement with several previous studies exploring the effect of crystallizing olivine, augite and plagioclase on silicate melt composition.

The liquid density is calculated by MELTS via a simplified polynomial representation of the liquid volumes, which uses estimates of the second pressure derivative of the molar volume and experimentally determined thermal expansivities and compressibilities for each liquid oxide [1]. Fig. 1e shows that the liquid density is constant when olivine is the only crystallizing phase. When pyroxene and plagioclase join the crystallization sequence the density increases, due to the FeO_{tot} enrichment in the liquid. This agrees with laboratory experiments [21] showing a liquid density increase during fractionation until iron oxides start to precipitate. Fig. 1e also shows that for a liquid of constant (initial) composition the density increases with decreasing temperature. Since the liquid density is a function of both temperature and composition, cooling and fractionation are not necessarily associated with decreasing liquid densities.

It is now interesting to go a step further and attempt to predict the composition of the residual liquid erupted at the surface. We consider two cases: In the 'one-stage case' fractionation occurs only at the Moho, the liquid then ascends to the surface along its liquidus gradient. Table 3 shows the liquid composition at 1220°C, which corresponds to an eruption temperature of 1200°C, if the liquid rises from $P_{Moho} = 3$ kbar to the surface along a liquidus gradient of ca. 7°C/kbar. The low SiO_2 and the high MgO concentrations are characteristic of a 'high-MgO basalt'.

For the 'two-stage case' we assume, arbitrarily, that 25 wt% fractionation occurs at the Moho and that the residual liquid further cools and fractionates at shallow pressure ($P = 1$ kbar). Table 3 shows the final composition of the liquid at $T = 1200$°C. Also in this case the liquid composition is that of a

Table 3
Final composition of the residual liquid

Oxide	IC-30 One stage $T = 1220$°C $P = 3$ kbar	IC-30 Two stage $T = 1200$°C $P = 1$ kbar	IC-20 One stage $T = 1220$°C $P = 3$ kbar	IC-20 Two stage $T = 1200$°C $P = 1$ kbar	IC-10 One stage $T = 1220$°C $P = 3$ kbar	IC-10 Two stage $T = 1200$°C $P = 1$ kbar
SiO_2	45.80	46.65	48.08	49.17	50.28	52.06
TiO_2	2.11	2.82	1.63	1.49	1.56	1.28
Al_2O_3	15.52	13.98	15.92	14.45	16.01	14.86
FeO_{tot}	14.04	14.12	12.91	12.35	11.22	10.01
Cr_2O_3	0.01	0.02	0.02	0.03	0.02	0.04
MgO	8.72	9.00	8.03	8.36	7.36	7.94
CaO	10.22	11.30	9.59	10.67	9.45	10.32
Na_2O	2.97	2.77	3.63	3.31	3.90	3.31
K_2O	0.15	0.14	0.18	0.16	0.22	0.18

'high-MgO basalt'. The solid phases fractionated at shallow pressure are olivine, clinopyroxene and plagioclase.

The results for the initial composition IC-20 are shown in Fig. 1, middle panels. The fractionated phases are olivine, followed at lower temperature by clinopyroxene and plagioclase (Fig. 1f), as expected the olivine content is less than for IC-30. The calculated P-wave velocity of the solid assemblage ranges from 8.5 km/s (for pure dunitic cumulus) to 7.4 km/s (Fig. 1g). Fig. 1h shows the MgO decrease in the residual liquid, due to olivine fractionation, and the effect of augite and plagioclase fractionation on FeO_{tot}, CaO, and Al_2O_3. The liquid density is relatively constant until pyroxene and plagioclase are formed (Fig. 1l).

The liquid composition for the one-stage model with initial composition IC-20 (Table 3) has SiO_2 48.08 wt% and MgO 8.03 wt% which is similar to observed compositions of hotspot erupted lavas. For the two-stage model (using the same constraints described above) the fractionated phases at $P = 1$ kbar are olivine and plagioclase, and the final liquid composition has higher SiO_2 (49.17 wt%) and MgO (8.36 wt%).

The results for the initial composition IC-10 are shown in Fig. 1 (bottom panels). As the temperature drops from the liquidus the fractionated phases are orthopyroxene, plagioclase and clinopyroxene (Fig. 1m). The calculated velocities of the solid assemblage range from 8.0 km/s to 7.0 km/s (Fig. 1n). Fig. 1o and 1p show the oxide concentration in the residual liquid, with the previously described trend induced by plagioclase and clinopyroxene fractionation. The liquid density increases as a consequence of the FeO_{tot} increase in the liquid (Fig. 1q).

The liquid composition for the one-stage model has SiO_2 50.28 wt% and MgO 7.36 wt% (Table 3). For the two-stage model the fractionated phases at $P = 1$ kbar are olivine and plagioclase, and the final liquid composition has SiO_2 52.06 wt% and MgO 7.94 wt%.

For the two stage model the relative volume proportions of the residual liquid and of the fractionated cumulus are shown in Fig. 2 (columns a, b, c). For the initial composition IC-30, 25 wt% fractionation at the Moho generates ultramafic cumulus (the volumetric proportion of Ol:Cpx:Pla:Sp is

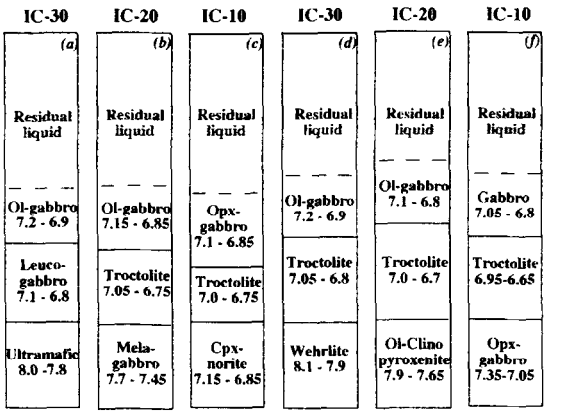

Fig. 2. Volume proportion of the solid phases and the residual liquid for the two-stage case. (a,b,c) Moho at $P = 3$ kbar. (d,e,f) Moho at $P = 5$ kbar. Numbers indicate the compressional velocity (km/s). Volume proportions are calculated from weight proportions using $\rho = 2.9$ g/cm^3, for mafic cumulates $\rho = 3.2$ g/cm^3. The dashed line is calculated assuming that 30% of the residual liquid is intruded.

67.5:16.5:13.5:2.5) with $V_P = 8.0$–7.8 km/s. For the initial composition IC-20 an olivine melagabbro is formed (Ol:Cpx:Pla:Sp is 40.7:28.5:28.5:2.3) with $V_P = 7.7$–7.45 km/s, while for the initial composition IC-10 a Cpx-norite is formed (Opx:Cpx:Pla:Sp is 25:16:58:1) with $V_P = 7.15$–6.85. It is interesting to note that the velocities of the fractionated cumulus are indeed different for the three initial compositions, and that high seismic velocities (7.8–7.4 km/s) are obtained only if the liquid reaching the Moho is picritic. The solid phases fractionated at low pressure ($P = 1$ kbar) are plagioclase and olivine, 80 and 20 volume percent respectively, and the corresponding V_P is 7.05–6.75 km/s. Only for IC-30 is there some augite: Ol:Cpx:Pla is 20:4:76, and thus $V_P = 7.1$–6.8 km/s. Our results indicate that the *coexistence* of high-velocity layers at the base of the crust with high upper crustal velocities is diagnostic of picritic mantle melts and indicative of deep primary melting.

After fractionation at the Moho and at $P = 1$ kbar the relative volume of the residual liquid is 56, 57 and 59%, respectively, for the IC-30, IC-20 and IC-10. However, it is likely that an unknown fraction of the remaining liquid will be intruded in the crust. We use the initial composition of the liquid reaching $P = 1$ kbar to find the composition of the 'intruded assemblage'. For equilibrium crystallization MELTS

calculates the solid phases formed until all the liquid is exhausted. In most cases the 'intruded' rock at $P = 1$ kbar is an olivine gabbro, with $V_P = 7.1–6.8$ km/s.

3.2. Moho at $P = 5$ kbar

We conducted the same set of calculations for an initial pressure of crystallization of 5 kbar. Since the stability field of olivine decreases with increasing pressure we expect a lower amount of fractionated olivine, as compared to the previous case. Fig. 2 (columns d, e, f) shows the relative volume proportions of the residual liquid and of the fractionated cumulus for the two stage model (i.e., fractionation at $P = 5$ kbar and $P = 1$ kbar) For the initial composition IC-30, 25 wt% fractionation at the Moho generates a wehrlite (the volumetric proportion of Ol:Cpx:Sp is 59:38:2.5) with $V_P = 8.1–7.9$ km/s. For the initial composition IC-20, an olivine clinopyroxenite is formed (Ol:Cpx:Sp is 30:67:3) with $V_P = 7.9–7.65$ km/s, while for the initial composition IC-10, an orthopyroxene gabbro is formed (Cpx:Opx:Pla:Sp is 49:11:39:1) with $V_P = 7.35–7.05$ km/s. We note that velocities of the fractionated cumulates are significantly different for the three initial compositions, and high seismic velocities (7.8–7.4 km/sec) are obtained only if the liquids reaching the Moho are picritic. The solid phases fractionated at low pressure ($P = 1$ kbar) are plagioclase and olivine, 80 and 20 vol.%, respectively, with $V_P = 7.0–6.7$ km/s. For all liquids at $P = 1$ kbar the corresponding intruded rocks are olivine gabbros, with $V_P = 7.1–6.8$ km/s. The final compositions of the residual liquids at $T = 1200$°C and $P = 1$ kbar are given in Table 4.

Table 4
Final composition of the residual liquid

Oxide	IC-30 Two stage $T = 1200$°C $P = 1$ kbar	IC-20 Two stage $T = 1200$°C $P = 1$ kbar	IC-10 Two stage $T = 1200$°C $P = 1$ kbar
SiO_2	46.68	48.57	52.28
TiO_2	1.81	1.59	1.31
Al_2O_3	13.87	14.47	14.85
FeO_{tot}	14.44	12.79	9.92
Cr_2O_3	0.02	0.02	0.03
MgO	8.88	8.33	7.87
CaO	11.31	10.57	10.23
Na_2O	2.86	3.50	3.32
K_2O	0.15	0.17	0.18

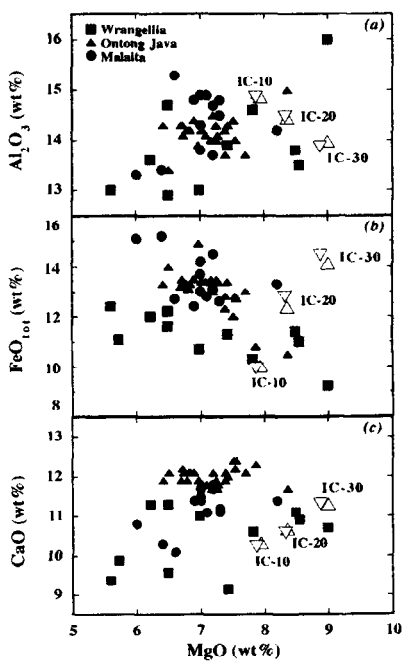

Fig. 3. MgO concentration vs. Al_2O_3 (a), FeO_{tot} (b), and CaO (c). Solid symbols: data from the Wrangellia terrane (squares), the Ontong Java plateau (triangles), Malaita island (circles). Open symbols: calculated liquid compositions (two-stage cases) for initial pressure of fractionation at 3 kbar (up-pointing triangles) and at 5 kbar (down-pointing triangles).

In Fig. 3 we compare the calculated major oxide concentrations in the liquid (for the two-stage cases) with the composition of basaltic rocks from (1) the Ontong Java plateau, noting that only the top 150 m of the plateau were sampled by Leg 130 [28], (2) the 'Older Series' at Malaita island, which is probably an obducted fragment of the Ontong Java plateau [29], and (3) the Wrangellia terrane, an accreted fragment of an oceanic plateau [8,9]. The comparison is satisfactory although some discrepancies are evident, for example, the calculated MgO concentration is higher than observed. The Al_2O_3 concentration for the two-stage case compares reasonably well with observations (Fig. 3a), plagioclase fractionation at low pressure reduces the exceedingly high Al_2O_3

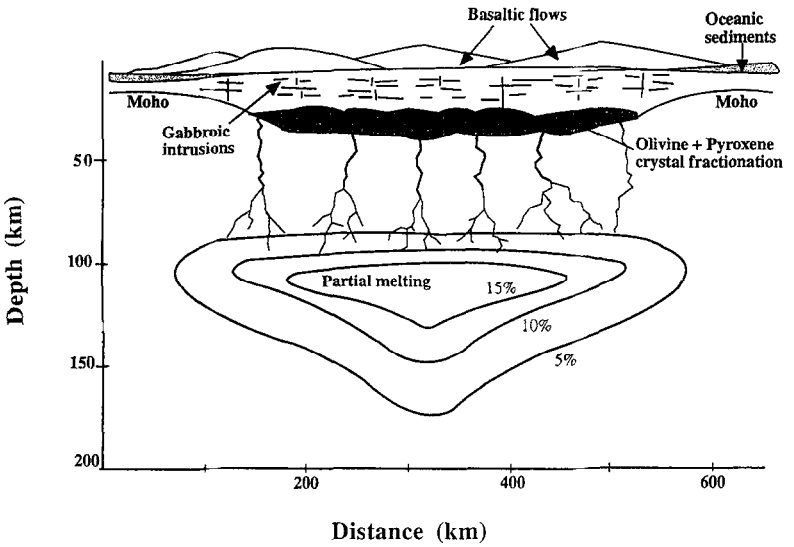

Fig. 4. Cartoon for the formation of an oceanic plateau.

concentrations predicted for the one-stage case. The differences in FeO_{tot} concentration among IC-10, IC-20 and IC-30 reflect the initial concentrations in the liquid, as expected FeO_{tot} is higher for partial melts formed at high initial pressure (Fig. 3b). The Mg# (Mg# = molar MgO/MgO + FeO) is 0.70, 0.68 and 0.64, for IC-30, IC-20 and IC-10, respectively, while basaltic lavas may have lower values (0.6–0.5) indicative of their evolved nature. Although the aim of our calculations was not to reproduce any particular observed lava composition, but instead to explore the effect of fractionation assuming plausible P–T paths, we note that the predicted final liquid compositions are in the range of observed basaltic lavas.

4. Discussion

In this paper we have modeled the petrological evolution of primary melts assuming that crystal fractionation is a fundamental process through which picritic melts evolve toward a basaltic composition. Our results suggest that high-velocity layers at the base of the crust represent mafic cumulates and that important intrusive magmatism is associated with volcanic activity at hotspots.

Our conceptual model is illustrated in Fig. 4. Partial melting occurs in the plume head at 70–120 km depths, as suggested by numerical models of convection/melting for plumes impinging on non-rifting oceanic lithosphere [11]. Melt migrates upward through porous flow or through veins toward the Moho. We assume that melts rise in the mantle along their liquidus. Major fractionation occurs at the base of the crust, where cumulate bodies of olivine, augitic clinopyroxene and plagioclase are formed. The fractionated cumulates are expected to have variable thickness and lenticular shapes, reflecting areas of higher partial melting in the plume, as well as rheological variations. Partial melts evolve toward a basaltic composition and rise through the crust, where intrusions of gabbros, variably enriched in olivine, contribute to crustal thickening. The residual liquid is then extruded as basalt flows.

4.1. Occurrence and nature of high-velocity basal crustal layers

Layers with high compressional velocities (V_p = 7.4–7.8 km/s) are occasionally observed in the lowermost crust in both continental and oceanic environments [30,31]. In continental settings high-velocity layers are associated with rift volcanism [32] and with rifted continental margins [33,34]. In extensional regimes crustal underplating is attributed to mantle melts ponding at the base of the continental crust [24].

In the oceanic environment layers with velocities intermediate between oceanic layer 3 (6.6–7.0 km/s) and the mantle (8.0–8.2 km/s) were discovered in the 1970's, but their origin was considered problematic. The anomalously high velocities were generally ascribed to upper mantle peridotites and dunites serpentinized by hydrothermal circulation, since serpentinization decreases the compressional velocity of ultramafic rocks. Other rock types with appropriate seismic velocity are amphybolites containing epidote and mafic garnet granulites (see [30] and references therein). High-velocity layers ($V_P = 7.4$ km/s and ~ 2 km thick) detected in some parts of the Atlantic Ocean, are interpreted as cumulate sequences formed at the floor of relatively persistent crustal magma chambers beneath spreading ridges [35]. In contrast the high-velocity layers detected beneath oceanic plateaus and hotspot tracks have a greater thickness (6–10 km) and seismic compressional wave velocities of 7.4–7.9 km/s, as described in more detail below.

Beneath the Shatsky rise reflection/refraction studies [36,37] identified the oceanic basement (3–6 km thick, $V_P = 4.7$–5.5 km/s), the main crustal layer ($V_P = 7.0$ km/s) and a basal layer 6–10 km thick, with V_P as high as 7.3–7.8 km/s. The crust is considerably thickened beneath the plateau, and the Moho is deeper than 22 km.

The crustal structure of the Ontong Java plateau was investigated by Furumoto et al. [15] with wide-angle reflection and refraction methods. In the northern part of the plateau they imaged a considerably thickened crust (~ 40 km), with a $V_P = 7.0$ km/s mid-crustal layer overlying a 7.6–7.7 km/s lower crust, 6–12 km thick. The crustal structure beneath the Ontong Java plateau is remarkably different from the adjacent basins, where the crust is ~ 15 km thick and high-velocity layers are absent.

Seismic refraction profiles beneath the Kerguelen Archipelago [38] identify the oceanic layer 2 (5–10 km thick, $V_P = 4.6$–4.8 km/s) and the oceanic layer 3 (6–8 km thick, $V_P = 6.6$–7.0 km/s). At the depth of 15–20 km the lowermost crustal seismic velocity is in the range 7.2–7.5 km/s for a layer 2–3 km thick. We note that the thickness of the high-velocity layer may have been underestimated, since compressional velocities as low as 7.8 km/s were attributed to the mantle.

Recent seismic reflection profiles of the Caribbean province [39], reveal the discontinuous presence of high-velocity layers at the base of the crust. Beneath the Beata Ridge layers with $V_P > 7.4$ km/s are up to 10 km thick, beneath the Columbia and the Haiti basin they are approximately 5 km thick, while in other areas they are not observed.

Seismic reflection beneath Hawaii [13] identify the upper crust ($V_P = 4.0$–7.0 km/s), the lower crust and a further reflector at the base of the crust beneath the island and flanking moats with $V_P = 7.4$–7.9 km/s. This high-velocity layer, ~ 4 km thick, has been attributed to ponding of mantle melts at the base of the crust [40].

Recent seismic refraction experiments across the Marquesas Islands hotspot trace [14] show a thickened crust (15–17 km) and a large lower-crustal region, 2–8 km thick, characterized by seismic velocities of 7.3–7.9 km/s. The upper mantle velocity is at least 8.1 km/s. Away from the platform the crust is 6 km thick and exhibits lower crustal velocities of 6.5–7.2 km/s. The high-velocity lower crustal body is indicative of large-scale crustal underplating of mafic and ultramafic rock that took place during hotspot volcanism [14]. Similarly, beneath the Reunion hotspot wide angle seismic data reveal high velocities at the base of the crust [41].

4.2. Models for the Ontong Java plateau

The Ontong Java plateau is the largest oceanic plateau on Earth, with an estimated volume of $\sim 50 \times 10^6$ km^3 [31]. The extensive magmatism which formed this plateau was probably induced by a mantle plume impinging on young (~ 20 Ma) oceanic lithosphere. The velocity–depth profile of the northern part of the plateau (Fig. 5a, from [15]) shows a ~ 35 km thick crust, with a 7.0 km/s mid-crustal layer (~ 15 km thick), overlying a 7.6–7.7 km/s lower crust (~ 12 km thick). The high compressional wave velocities in the uppermost mantle (8.4–8.6 km/s) could be imprecise, being determined only from second arrivals.

The predicted crustal structure (Fig. 5b) is calculated assuming that major fractionation occurs at the Moho, but, in contrast to the previous cases, we allow some fractionation also in the uppermost mantle. As the picritic melt (IC-30) is en route from 8

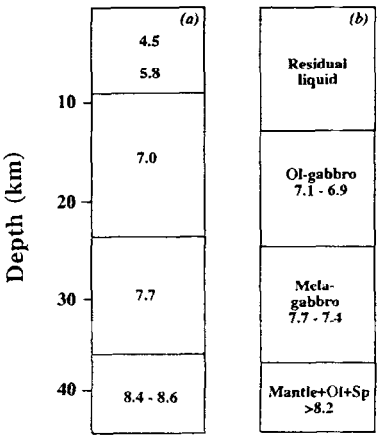

Fig. 5. (a) Crustal structure of the northern part of the Ontong Java Plateau (line Q, [15]). Numbers indicate the compressional velocities (km/s). The uppermost 3.2 km of sediments are not shown. (b) Calculated crustal structure.

kbar to the Moho (P = 3 kbar) it fractionates 10 wt% of olivine and spinel (the volume ratio is 94:6 and $V_P = 8.4$ km/s). Fractionation at the Moho generates cumulates of melagabbro (ol:cpx:pla is 43:27:30) with $V_P = 7.7–7.4$ km/s. The phases fractionated in the upper crust ($P = 1$ kbar) are olivine and plagioclase ($V_P = 7.0–6.7$ km/s), while crustal intrusions are olivine gabbros ($V_P = 7.1–6.9$ km/s).

This model is simplistic, since neither the primary melt composition, nor the depth of fractionation are likely to remain constant during the plateau formation; however, it predicts a distinct crustal structure. (1) In the uppermost mantle olivine and spinel enrichment may explain the unusually high seismic velocities. (2) At the base of the crust fractionated cumulates of melagabbro have high seismic velocities, well in the range of measured lower crustal elocities of the Ontong Java plateau. (3) In the upper crust magmatic intrusions of olivine gabbro have relatively high seismic velocities of ~ 7.0 km/s.

In this model 25 wt% fractionation at the Moho is followed by 5 wt% fractionation in shallow magma chambers, therefore the remaining liquid is 70 wt% of the mantle melts reaching the Moho. In such case the 'layer of erupted basalts' should be much thicker than the underlying crustal layers. The seismic structure beneath the Ontong Java plateau indicates exactly the opposite, since the deep crustal layers ($V_P = 6.8–7.7$ km/s) are much thicker than the uppermost 'basaltic' layer ($V_P = 4.5–5.8$ km/s). In order to approximate the observed relative thickness we need to hypothesize that the crust is thickened also by 'intrusions', either in the form of intruded mafic bodies, or as frozen sills and dykes. If we assume 5 wt% intrusion at the base of the crust and 25 wt% intrusion in the upper crust, then the residual liquid is only 40 wt% of the magma reaching the Moho. In this case the relative thickness (Fig. 5b) compare reasonably well with the observations. Note that (1) we neglected the contribution of the young oceanic crust present at the time of the plateau formation, (2) the high-velocity layers may be restricted to the central part of the plateau, therefore their extent may not coincide with the area covered by lava flows. Although this model is only qualitative it suggests that extruded basalts are accompanied by even greater volumes of underplated and intruded igneous rocks.

4.3. Are the high-velocity layers garnet granulites?

The discovery of mafic garnet granulite xenoliths at Kerguelen Island has lead to the alternative suggestion that high seismic velocities at the base of the crust are due to the presence of garnet granulite [42]. In this case the isochemical transformation of crustal gabbros into garnet granulites (i.e., cpx + opx + pla + garnet) induces high seismic velocities. Although solid phase transitions proceed at different pressures and to differing degrees depending on the bulk composition, on the geothermal gradient and on the availability of fluids, we would expect the plagioclase–garnet transformation to occur at a fairly constant depth range.

For the Ontong Java plateau the available seismic profiles indicate that at a constant depth the compressional velocities can differ significantly. For example, at 35 km depth the velocities are 6.9 km/s (lines P and W) and 7.6–7.7 km/s (lines R and Q [15]). Moreover, the depth of the high-velocity layers varies considerably among provinces: it is ~ 30 km beneath the Ontong Java plateau, but is only ~ 12–16 km beneath hotspots. It seems rather unlikely that these significant depth variations are due solely to solid phase transformations.

We do not rule out the occurrence of phase transformations in the deep crust, mainly beneath the

deep Ontong Java plateau, but we suggest that the plagioclase–garnet transformation is not a sufficient mechanism to consistently explain the origin of the high-velocity layers beneath oceanic plateaus and hotspot tracks. We also note that according to our model the high-velocity layers are more mafic and less aluminous than the overlying gabbros, so that the plagioclase–garnet transformation may not have such a profound effect.

5. Conclusions

We used the petrological code MELTS to model the compositional evolution of deep mantle plume melts, assuming that crystal fractionation is the dominant mechanism through which picritic liquids evolve toward a basaltic composition. We focused on the effect that crystal fractionation may have on the crust and uppermost mantle structure, and we compared model predictions with crustal structures seismically imaged beneath some oceanic plateaus and hotspot tracks.

We assumed that mantle melts pond, cool and fractionate at the base of the crust. Our initial liquid compositions span a range of primary melts representative of deep melting (30–20 kbar pressure), and shallow melting (10 kbar). For the three initial liquids, the cumulates fractionated at the Moho have significantly different bulk compositions and compressional wave velocities. For example, at 25 wt% fractionation, the cumulates formed from deep primary melts (IC-30 and IC-20) are ultramafic rocks ($V_P = 8.0$–7.8 km/s) and melagabbros (7.7–7.4 km/s), respectively, while for shallow primary melts the cumulates are gabbros (7.1–6.8 km/s). These results suggest that high-velocity layers (7.9–7.4 km/s) detected at the base of the crust beneath oceanic plateaus and hotspot tracks are associated with plume volcanism and may represent fractionated cumulates from picritic mantle melts formed in the uppermost mantle.

In our models upper crustal intrusions are generally olivine gabbros (7.1–6.85 km/s), while additional crystal fractionation at $P = 1$ kbar, generates troctolites (7.0–6.75 km/s). At surface conditions ($T = 1200$°C) the final liquid compositions are in the range of what is observed for flood basalt lavas, and the ratio SiO_2/MgO is 46.7/9.0, 49.2/8.4 and 52.1/7.9, respectively, for IC-30, IC-20 and IC-10.

We have also attempted to explain the crustal structure of the Ontong Java plateau. In this case we allowed some crystal fractionation in the uppermost mantle. As the picritic melt is en route to the Moho, the fractionated phases are olivine and spinel, which have high compressional velocities. Further fractionation at the base of crust generates cumulates of melagabbro, with calculated compressional velocities of 7.7–7.4 km/s, similar to the observed velocities beneath the plateau. Upper crustal intrusions are olivine gabbro, with relatively high seismic velocities ($\sim$ 7.0 km/s).

We suggest that the high-velocity layers detected at the base of the crust beneath oceanic plateaus and hotspot tracks are an integral part of plume volcanism, since they represent fractionated cumulates from picritic mantle melts. Therefore, we also predict the existence of high-velocity bodies and crustal thickening beneath continental flood basalt provinces. Interestingly, beneath the central area of the Columbia River Flood basalt, Catchings and Mooney [16] identified a high-velocity body (7.5 km/s) overlying a fast upper mantle (8.4 km/s). This layer, $\sim$ 15 km thick, was interpreted as a 'rift pillow', but we suggest that it may represent a cumulate body of fractionated olivine and clinopyroxene related to the Columbia River basalts. We are not aware of any detailed seismic studies of deep crustal structure beneath other continental flood basalt provinces or where volcanism did not occur by decompressional melting at rifted margins. Our results show that further studies of the deep crustal seismic structure beneath large igneous provinces may be diagnostic of the processes through which primary mantle melts evolve prior to eruption.

Acknowledgements

We thank an anonymous reviewer, Marc Hirschmann, Norman Sleep and Dan McKenzie for thorough and constructive reviews of the paper. We also thank Mike Coffin for useful discussions. This research was supported by NSF grant EAR9057012 awarded to M.A.R. *[FA]*

References

[1] M.S. Ghiorso and R.O. Sack, Chemical mass transfer in magmatic processes, IV. A revised and internally consistent thermodynamic model for the interpolation and extrapolation of liquid–solid equilibria in magmatic systems at elevated temperatures and pressures, Contrib. Mineral. Petrol. 119, 197–212, 1995.

[2] W.J. Morgan, Plate motions and deep mantle convection, Mem. Geol. Soc. Am. 132, 7–22, 1972.

[3] W.J. Morgan, Hotspot tracks and the opening of the Atlantic and Indian Oceans, in: The Sea, Vol. 7. The Oceanic Lithosphere, C. Emiliani, ed., pp. 443–487, Wiley, New York, NY, 1981.

[4] M.A. Richards, R.A. Duncan and V.E. Courtillot, Flood basalts and hotspot tracks: plume heads and tails, Science 246, 103–107, 1989.

[5] I.H. Campbell and R.W. Griffiths, Implications of mantle plume structure for the evolution of flood basalts, Earth Planet. Sci. Lett. 99, 79–93, 1990.

[6] K.W.W. Sims, D.J. DePaolo, M.T. Murrell, W.S. Baldridge, S.J. Goldstein and D.A. Clague, Mechanism of magma generation beneath Hawaii and mid-ocean ridges: uranium/thorium and samarium/neodymium isotopic evidence, Science 267, 508–512, 1995.

[7] J.L. Wooden et al. Isotopic and trace-element constraints on mantle and crustal contributions to Siberian continental flood basalts, Norilsk area, Siberia, Geochim. Cosmochim. Acta 57, 3677–3704, 1993.

[8] J.C. Lassiter, D.J. DePaolo and J.J. Mahoney, Geochemistry of the Wrangellia flood basalt province: Implications for the role of continental and oceanic lithosphere in flood basalt genesis, J. Petrol. 36, 983–1009, 1995.

[9] M.A. Richards, D.L. Jones, R.A. Duncan and D.J. DePaolo, A mantle plume initiation model for the Wrangellia flood basalt and other oceanic plateaus, Science 254, 263–267, 1991.

[10] N.T. Arndt and U. Christensen, The role of lithospheric mantle in continental flood volcanism: thermal and geochemical constraints, J. Geophys. Res. 97, 10,967–10,981, 1992.

[11] C.G. Farnetani and M.A. Richards, Numerical investigation of the mantle plume initiation model for flood basalt events, J. Geophys. Res. 99, 13813–13833, 1994.

[12] K.G. Cox, A model for flood basalt vulcanism, J. Petrol. 21, 629–650, 1980.

[13] A.B. Watts and U.S. ten Brink, Crustal structure, flexure and subsidence history of the Hawaiian Islands, J. Geophys. Res. 94, 10473–10500, 1989.

[14] D.V. Caress, M.K. McNutt, R.S. Detrick and J.C. Mutter, Seismic imaging of hotspot-related crustal underplating beneath the Marquesas Islands, Nature 373, 600–603, 1995.

[15] A.S. Furumoto, J.P. Webb, M.E. Odegard and D.M. Hussong, Seismic studies on the Ontong Java Plateau, 1990, Tectonophysics 34, 71–90, 1976.

[16] R.D. Catchings and W.D. Mooney, Crustal structure of the Columbia Plateau: evidence for continental rifting, J. Geophys. Res. 93, 459–474, 1988.

[17] K. Hirose and I. Kushiro, Partial melting of dry peridotites at high pressures: determination of compositions of melts segregated from peridotite using aggregates of diamond, Earth Planet. Sci. Lett. 114, 477–489, 1993.

[18] E. Stolper and D. Walker, Melt density and average composition of basalt, Contrib. Mineral. Petrol. 74, 7–12, 1980.

[19] T. Parsons, N.H. Sleep and G.A. Thompson, Host rock rheology controls on the emplacement of tabular intrusions: implications for underplating of extending crust, Tectonics 11, 1348–1356, 1992.

[20] R.A. Lange and I.S.E. Carmichael, Thermodynamic properties of the silicate liquids with emphasis on density, thermal expansion and compressibility, in: Modern Methods of Igneous Petrology: Understanding Magmatic Processes, J. Nicholls and J.K. Russell, eds., pp. 25–59, Reviews in Mineralogy, 24, Mineral. Soc. of America, Washington DC, 1990.

[21] V.C. Kress and I.S.E. Carmichael, The compressibility of silicate liquids containing Fe_2O_3 and the effect of composition, temperature, oxygen fugacity and pressure on their redox states, Contrib. Mineral. Petrol. 108, 82–92, 1991.

[22] M.B. Baker, M.M. Hirschmann, E.M. Stolper and M.S. Ghiorso, Compositions of low-degree partial melts of peridotite: Results from experiments and thermodynamic calculations, Nature 375, 308–311, 1995.

[23] N.I. Christensen, in: Handbook of Physical Properties of Rocks, R.S. Carmichael, ed., pp. 2–228, CRC Press Inc., Florida, 1982.

[24] K.P. Furlong and D.M. Fountain, Continental crustal underplating: Thermal considerations and seismic–petrological consequences, J. Geophys. Res. 91, 8285–8294, 1986.

[25] P.R. Hooper, Physical and chemical constraints on the evolution of the Columbia River basalt, Geology, 12, 495–499, 1984.

[26] M.P. Ryan, R.Y. Koyanagi and R.S. Fiske, Modeling the three-dimensional structure of macroscopic magma transport systems: application to Kilauea volcano, Hawaii, J. Geophys. Res. 86, 7111–7129, 1981.

[27] J.W. Elder, Magma traps, Part I. Theory, in: Pageoph. 117, Contributions to Current Research in Geophysics, L. Rybach and Stegena L., eds., 7, 3–14, 1979.

[28] J.J. Mahoney, M. Storey, R.A. Duncan, K.J. Spencer and M. Pringle, 1. Geochemistry and geochronology of Leg 130 basement lavas: nature and origin of the Ontong Java plateau, Proc. Ocean Drill. Progr., Sci. Results 130, 3–22, 1993.

[29] M.L.G. Tejada, J.J. Mahoney, R.A. Duncan and M.P. Hawkins, Age and geochemistry of basement and alkalic rocks of Malaita and Santa Isabel, Solomon Islands, southern margin of the Ontong Java plateau, J. Petrol. 37, 361–394, 1996.

[30] R.L. Carlson, N.I. Christensen and R.P. Moore, Anomalous crustal structure in ocean basins: continental fragments and oceanic plateaus, Earth Planet. Sci. Lett. 51, 171–180, 1980.

[31] M.F. Coffin and O. Eldholm, Large igneous provinces: crustal structure, dimensions, and external consequences, Rev. Geophys. 32, 1–36, 1994.

[32] C.M. Jarchow, G.A. Thompson, R.D. Catchings and W.D.

Mooney, Seismic evidence for active magmatic underplating beneath the Basin and Range Province, Western United States, J. Geophys. Res. 98, 22095–22108, 1993.

[33] W.S. Holbrook and P.B. Kelemen, Large igneous provinces on the United States Atlantic margin and implications for magmatism during continental breakup, Nature 364, 433–436, 1993.

[34] R.S. White, G.D. Spence, S.R. Fowler, D.P. McKenzie, G.K. Westbrook and A.N. Bowen, Magmatism at rifted continental margins, Nature 330, 439–444, 1987.

[35] J.C. Mutter, Multichannel seismic images of the oceanic crust's internal structure: evidence for a magma chamber beneath the Mesozoic Mid-Atlantic ridge, Geology 13, 629–632, 1985.

[36] N. Den et al. Seismic-refraction measurements in the northwest pacific basin, J. Geophys. Res. 74, 1421–1434, 1969.

[37] L.I. Kogan, Crustal structure of the Shatsky Rise in the northwestern Pacific, from deep seismic reflection profiling, Dokl, Acad. Sci. USSR Earth Sci. Sect., English Transl. 258, 25–30, 1981.

[38] M. Recq, D. Brefort, J. Malod and J.L. Veinante, The Kerguelen Isles (southern Indian Ocean): new results on deep structure from refraction profiles, Tectonophysics 182, 227–248, 1990.

[39] A. Mauffret and S. Leroy, Seismic stratigraphy and structure of the Caribbean Igneous Province, Tectonophysics, submitted, 1996.

[40] U.S. ten Brink and T.M. Brocher, Multichannel seismic evidence for a subcrustal intrusive complex under Oahu and a model for Hawaiian volcanism, J. Geophys. Res. 92, 13687–13707, 1987.

[41] L.A. Driad, Hirn, A. Nercessian, P. Charvis, A. Laesanpura and J. Gallart, Crustal and upper mantle structure under the Reunion hotspot from seismic wide angle data, Eos Trans. AGU 95, Fall Meeting Suppl. 587, 1995.

[42] M.N. Gregoire, Mattinelli, C. Nicollet, J.Y. Cottin, H. Leyrit, N. Shimizu and A. Giret, Oceanic mafic granulite xenoliths from the Kerguelen archipelago, Nature 367, 360–363, 1994.